Supporting Information for

Nearly one-fold enhancement in photoluminescence quantum yield for isostructural zero-dimensional hybrid antimony(III) bromides by supramolecular interactions adjustment

Ying-Chen Peng,[a,c] Sheng-Hua Zhou,[a,c] Jian-Ce Jin,[a,c] Qi Gu,[a,c] Ting-Hui Zhuang,[a] Liao-Kuo Gong,[a] Ze-Ping Wang,[a] Ke-Zhao Du,[b]* Xiao-Ying Huang[a,c]*

[a] State Key Laboratory of Structure Chemistry, Fujian Institute of Research on the Structure of Matter, Chinese Academy of Sciences, Fuzhou 350002, China.
[b] College of Chemistry and Materials Science, Fujian Provincial Key Laboratory of Polymer Materials, Fujian Normal University, 32 Shangsan Road, Fuzhou 350007, China.
[c] University of Chinese Academy of Sciences, Beijing, 100049, China.

Table S1. Crystal data and structure refinement for $[EtPPh_3]_2[SbBr_5]$·EtOH (**1·EtOH-Br**) at 293 K and $[EtPPh_3]_2[SbBr_5]$·MeCN (**1·MeCN-Br**) at 295 K.

	1·EtOH-Br	**1·MeCN-Br**
CCDC number	218160	218161
Empirical formula	$C_{42}H_{46}Br_5OP_2Sb$	$C_{42}H_{43}Br_5NP_2Sb$
Formula weight	1150.03	1145.01
Temperature/K	293(2)	295(2)
Wavelength/Å	0.71073	0.71073
Crystal system	Monoclinic	Monoclinic
Space group	*C*2/*c*	*C*2/*c*
a/Å	22.569(2)	22.833(2)
b/Å	16.6933(16)	16.9477(14)
c/Å	13.6310(12)	13.4634(12)
α/°	90	90
β/°	120.949(8)	121.633(8)
γ/°	90	90
Volume/Å^3	4404.4(8)	4435.9(7)
Z	4	4
ρ_{calc} g/cm^3	1.734	1.715
Absorption coefficient/mm^{-1}	5.266	5.227
F(000)	2248	2232
Crystal size/mm^3	0.600×0.400×0.400	0.200×0.180×0.150
Theta range for data collection /°	2.440-29.783	2.095-29.815
Limiting indices	-31<=*h*<=28, -23<=k<=19, -18<=*l*<=17	-29<=*h*<=31, -23<=*k*<=23, -16<=*l*<=17
Reflections collected/ unique	12260/5226 [R_{int} = 0.0473]	25127/5748 [R_{int} = 0.0523]
Completeness to theta	25.242, 99.9 %	25.242, 100.0 %
Absorption correction	Semi-empirical from equivalents	Semi-empirical from equivalents
Max. transmission	1.00000	1.00000
Min. transmission	0.27236	0.19319
Refinement method	Full-matrix least-squares on F^2	Full-matrix least-squares on F^2
Data/restraints/parameters	5226/2/248	5748/0/247
Goodness-of-fit on F^2	1.004	1.015
Final *R* indexes [$I >= 2\sigma(I)$]	R_1 = 0.0435, wR_2 = 0.0769	R_1 = 0.0367, wR_2 = 0.0679
Final *R* indexes [all data]	R_1 = 0.0776, wR_2 = 0.0903	R_1 = 0.0866, wR_2 = 0.0845
Extinction coefficient	0.00106(5)	n/a
Largest diff. peak and hole/e Å^{-3}	0.769/-0.914	0.614/-0.789

[a] $R_1 = \sum \| F_o | - | F_c \| / \sum | F_o |$, [b] $wR_2 = [\sum w(F_o^2 - F_c^2)^2 / \sum w(F_o^2)^2]^{1/2}$

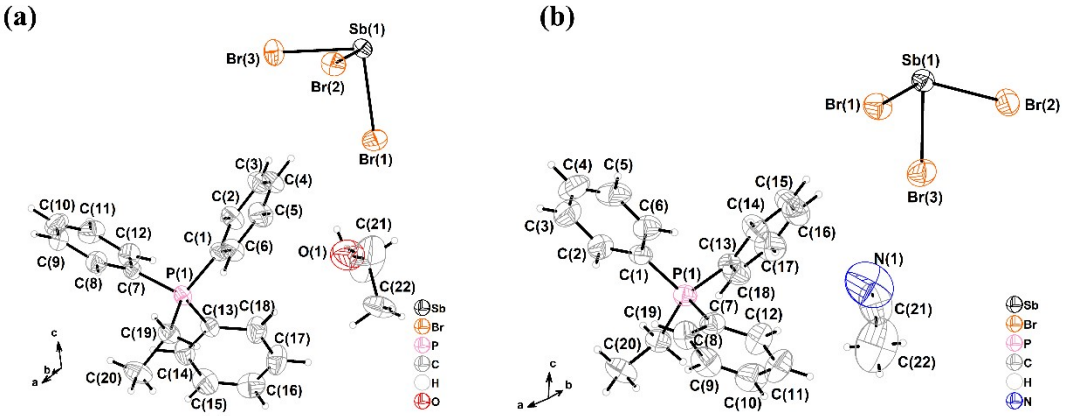

Figure S1. *ORTEP* drawings (50% ellipsoid probability) of the asymmetric units of $[EtPPh_3]_2[SbBr_5]\cdot EtOH$ (**1·EtOH-Br**) at 293 K (**a**) and $[EtPPh_3]_2[SbBr_5]\cdot MeCN$ (**1·MeCN-Br**) at 295 K (**b**).

Table S2. Selected bond lengths (Å) and bond angles (°) for $[EtPPh_3]_2[SbBr_5]\cdot EtOH$ (**1·EtOH-Br**) at 293 K and $[EtPPh_3]_2[SbBr_5]\cdot MeCN$ (**1·MeCN-Br**) at 295 K.

1·EtOH-Br		**1·MeCN-Br**	
Sb(1)-Br(1)	2.5174(8)	Sb(1)-Br(1)	2.5196(7)
Sb(1)-Br(3)#1	2.7716(5)	Sb(1)-Br(3)	2.7643(5)
Sb(1)-Br(3)	2.7717(5)	Sb(1)-Br(3)#1	2.7644(5)
Sb(1)-Br(2)	2.7769(5)	Sb(1)-Br(2)#1	2.7753(5)
Sb(1)-Br(2)#1	2.7770(5)	Sb(1)-Br(2)	2.7754(5)
Br(1)-Sb(1)-Br(3)#1	91.620(13)	Br(1)-Sb(1)-Br(3)	90.797(12)
Br(1)-Sb(1)-Br(3)	91.619(13)	Br(1)-Sb(1)-Br(3)#1	90.797(12)
Br(3)#1-Sb(1)-Br(3)	176.76(3)	Br(3)-Sb(1)-Br(3)#1	178.41(2)
Br(1)-Sb(1)-Br(2)	88.363(12)	Br(1)-Sb(1)-Br(2)#1	89.004(11)
Br(3)#1-Sb(1)-Br(2)	91.329(17)	Br(3)-Sb(1)-Br(2)#1	91.453(16)
Br(3)-Sb(1)-Br(2)	88.764(17)	Br(3)#1-Sb(1)-Br(2)#1	88.576(16)
Br(1)-Sb(1)-Br(2)#1	88.362(12)	Br(1)-Sb(1)-Br(2)	89.003(11)
Br(3)#1-Sb(1)-Br(2)#1	88.764(17)	Br(3)-Sb(1)-Br(2)	88.575(16)
Br(3)-Sb(1)-Br(2)#1	91.328(17)	Br(3)#1-Sb(1)-Br(2)	91.451(17)
Br(2)-Sb(1)-Br(2)#1	176.73(2)	Br(2)#1-Sb(1)-Br(2)	178.01(2)

Symmetry transformations used to generate equivalent atoms: #1 $-x+1, y, -z+3/2$

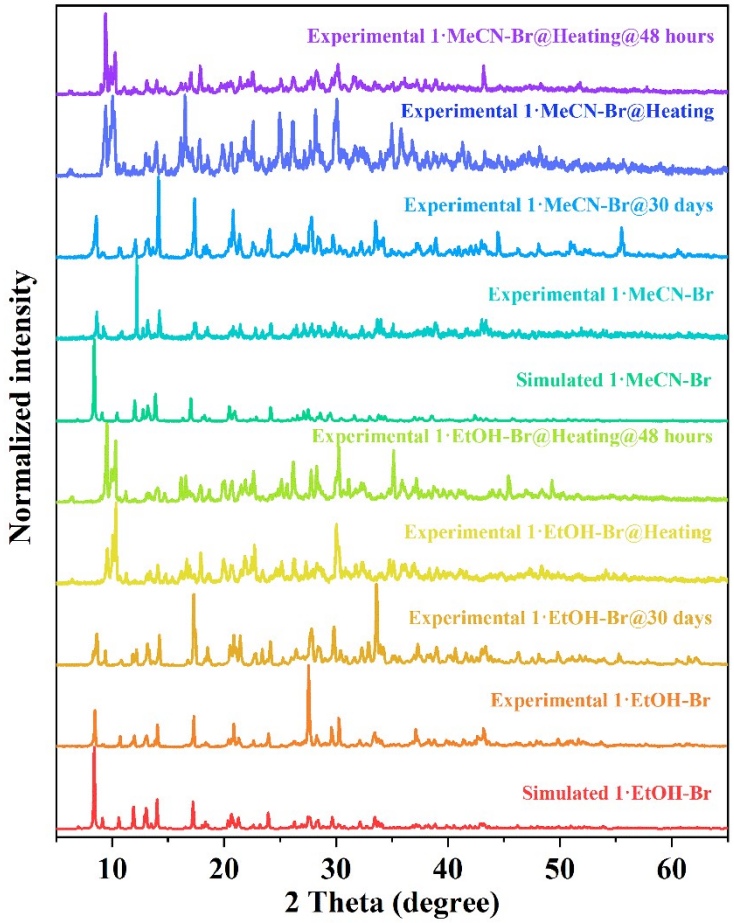

Figure S2. Simulated and experimental (including freshly prepared samples, samples staying for 30 days, samples after heating for desolvation and solvent-loss samples after staying for 48 hours) PXRD patterns of **1·EtOH-Br** and **1·MeCN-Br** at RT.

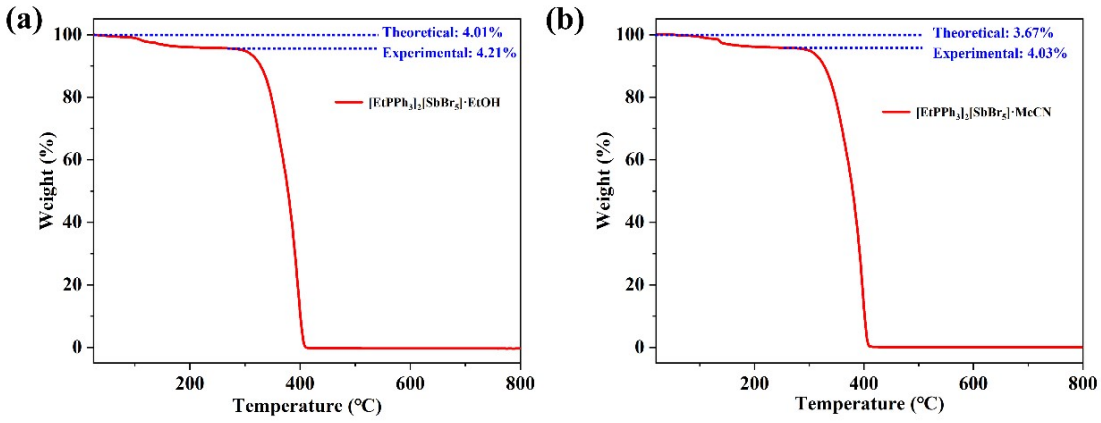

Figure S3. TG curves of **1·EtOH-Br** (**a**) and **1·MeCN-Br** (**b**).

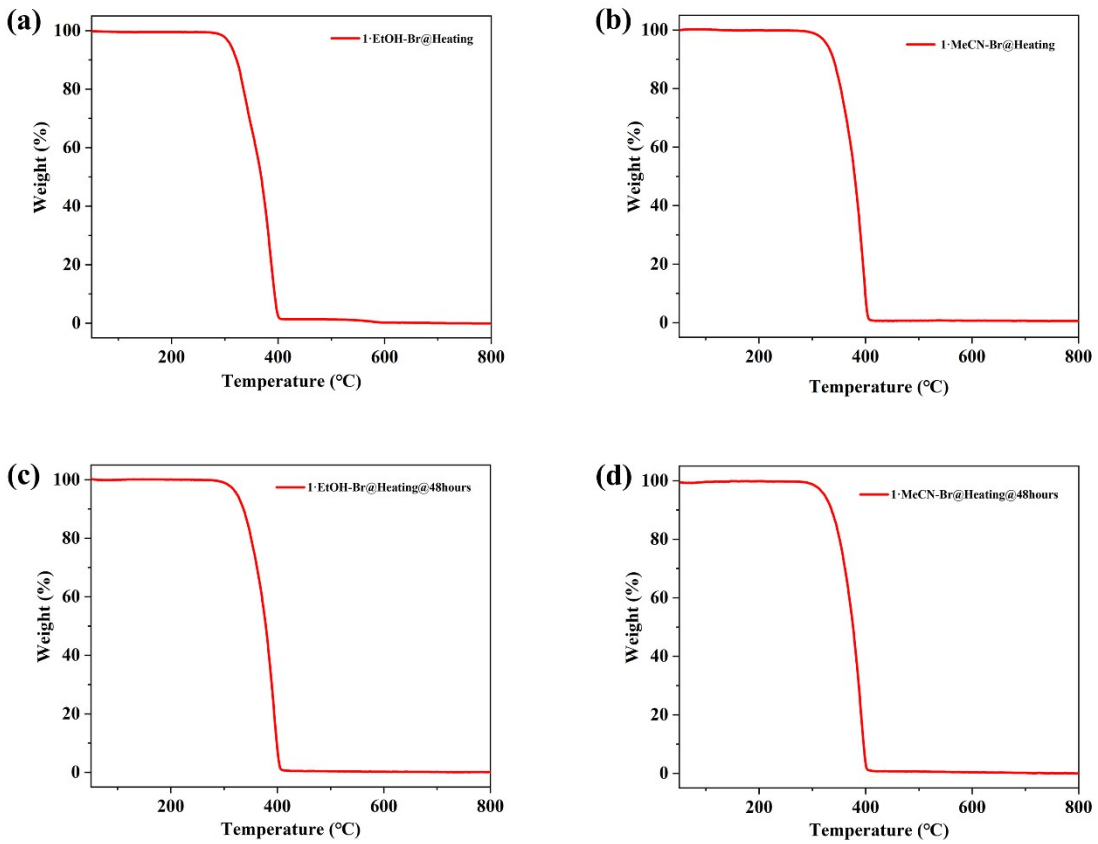

Figure S4. TG curves of **1-Br** from heating **1·EtOH-Br** (**a**) and **1·MeCN-Br** (**b**). TG curves for the **1-Br** samples from heating **1·EtOH-Br** (c) and **1·MeCN-Br** (d) being re-tested after 48 hours in ventilation closet.

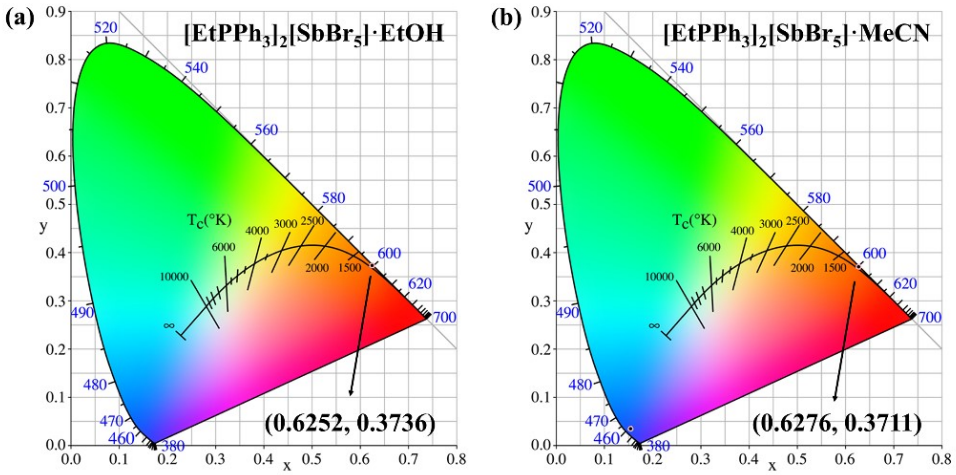

Figure S5. The Commission Internationale del'Eclairage (CIE) (1931) chromaticity coordinates of **1·EtOH-Br** (**a**) and **1·MeCN-Br** (**b**).

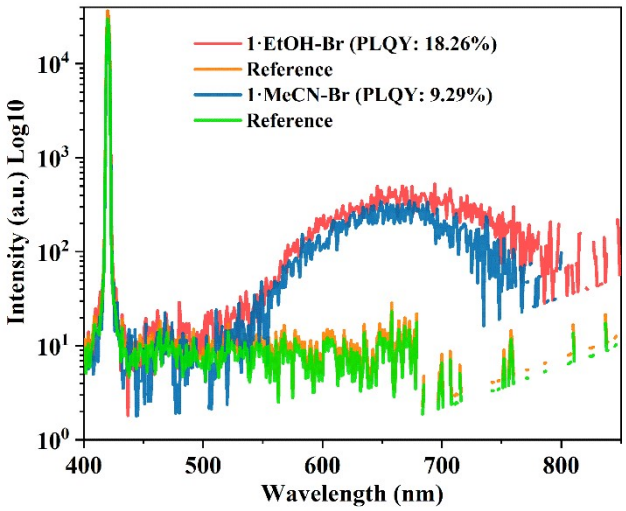

Figure S6. PLQY of **1·EtOH-Br** and **1·MeCN-Br**.

Table S3. The fitting parameters in the function based on the time-resolved PL spectra data of **1·EtOH-Br** and **1·MeCN-Br**.

	1·EtOH-Br	**1·MeCN-Br**
Function	$I = A_1exp(-t/T_1) + A_2exp(-t/T_2) + y_0$	
A_1	0.88356 ± 0.01532	0.90798 ± 0.06392
A_2	0.02505 ± 0.0153	0.11026 ± 0.06443
T_1	0.41182 ± 0.00486	0.2398 ± 0.00715
T_2	1.18908 ± 0.45274	0.46035 ± 0.10426
y_0	6.08584E-4 ± 6060066E-4	4.91358E-4 ± 6.1821E-4
Adj. *R* Square	0.99778	0.99804

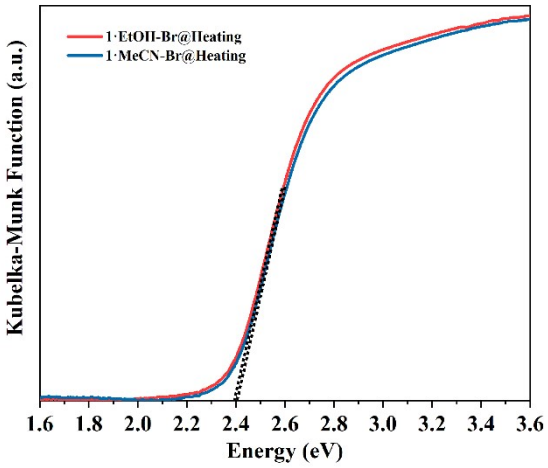

Figure S7. UV-vis spectra of **1-Br** from heating **1·EtOH-Br** and **1·MeCN-Br**, respectively.

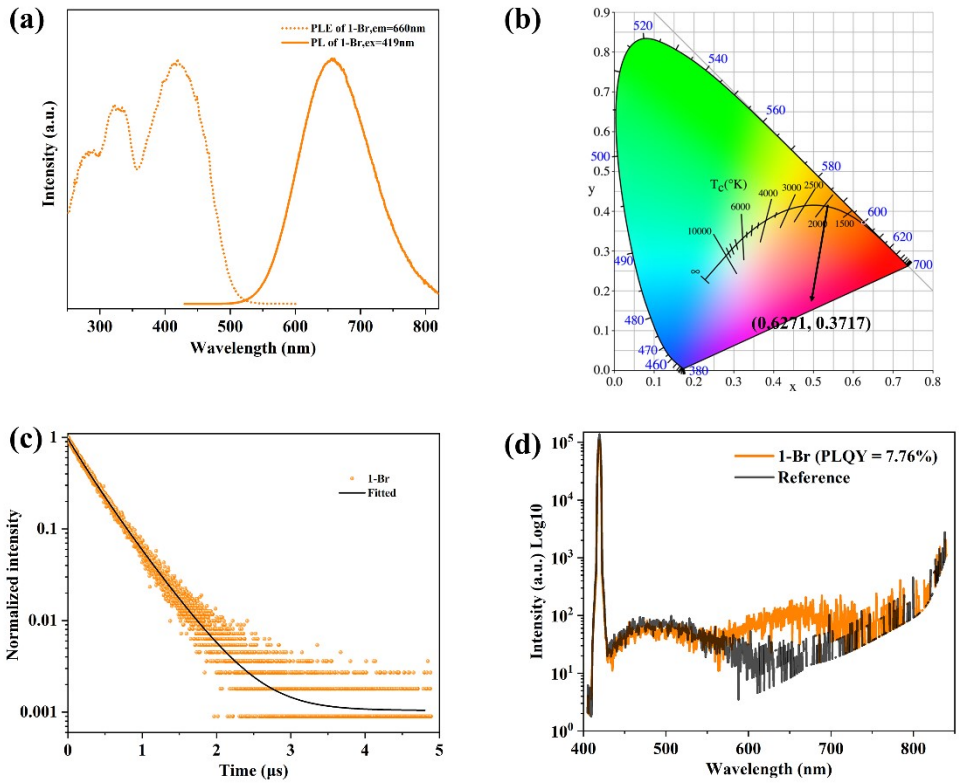

Figure S8. Steady-state PLE and PL spectra of **1-Br** (emission peak at 660 nm) under 419 nm excitation at RT (**a**). The CIE chromaticity coordinate of**1-Br** (**b**). Time-resolved PL decay curves of **1-Br** at RT (**c**). PLQY of **1-Br** (**d**).

Table S4. The fitting parameters in the function based on the time-resolved PL spectra data of **1-Br**.

	1-Br
Function	
A_1	0.37742 ± 0.0753
A_2	0.59393 ± 0.0759
T_1	0.23815 ± 0.01537
T_2	0.41233 ± 0.01364
y_0	0.00104 ± 1.836E-4
Adj. *R* Square	0.99782

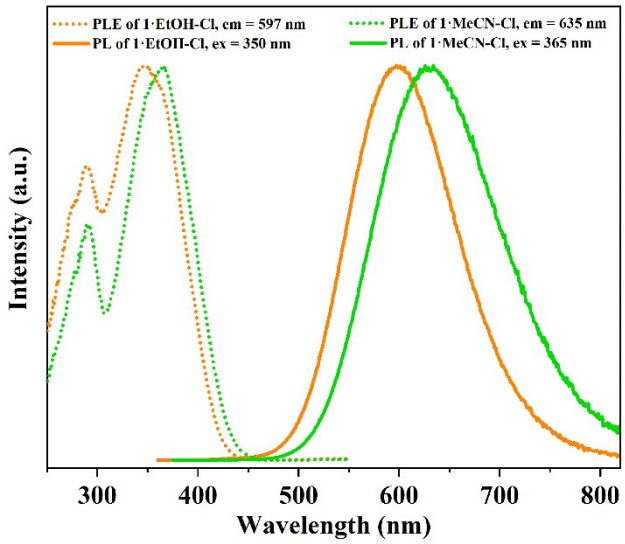

Figure S9. The steady-state PLE and PL spectra of **1·EtOH-Cl** (emission peak at 597 nm) and **1·MeCN-Cl** (emission peak at 634 nm) under excitation of 350 and 365 nm at RT, respectively.

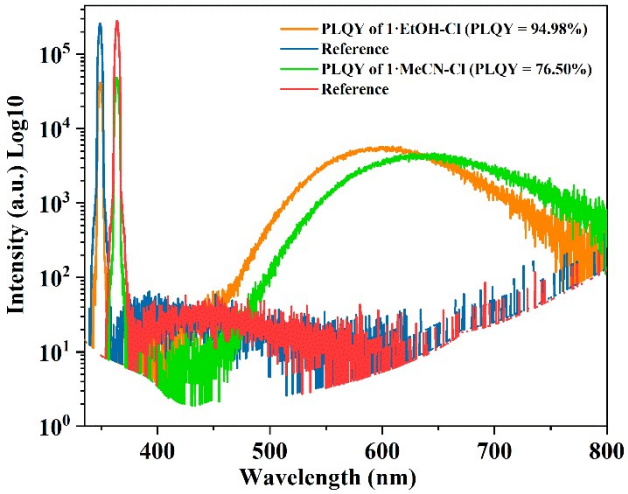

Figure S10. PLQY of **1·EtOH-Cl** and **1·MeCN-Cl**.

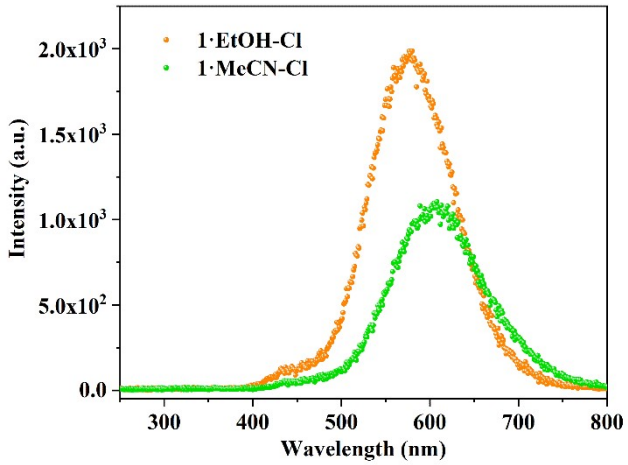

Figure S11. The XEL spectra of **1·EtOH-Cl** and **1·MeCN-Cl**.

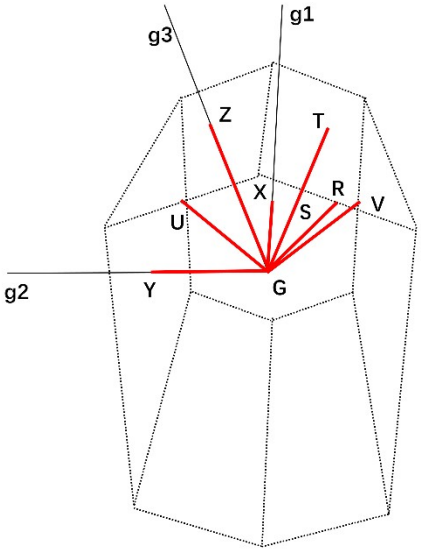

Figure S12. The first Brillouin zone with high symmetry points of **1·MeCN-Br**.

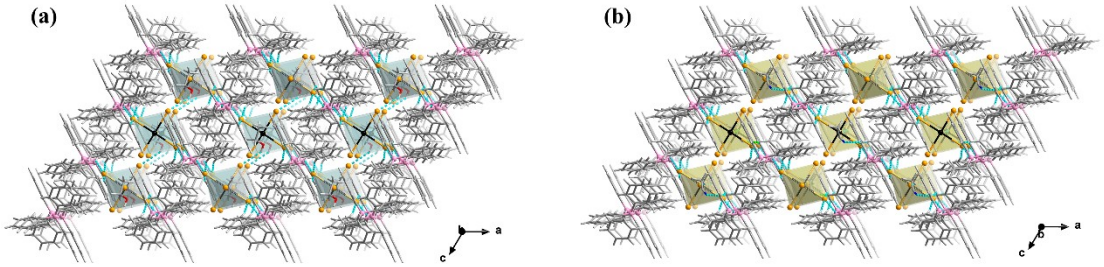

Figure S13. Diagrams of supramolecular structures of **1·EtOH-Br** (**a**) and **1·MeCN-Br** (**b**). Black ball, Sb; light orange ball, Br; blue ball, N; red ball, O; dark gray ball, C; light gray ball, H.

Table S5. Hydrogen bonds for $[EtPPh_3]_2[SbBr_5]\cdot EtOH$ (**1·EtOH-Br**) at 293 K and $[EtPPh_3]_2[SbBr_5]\cdot MeCN$ (**1·MeCN-Br**) at 295 K.

D-H···A	d(D-H)	d(H···A)	d(D···A)	<(DHA)
1·EtOH-Br				
C(2)-H(2)···Br(2)#2	0.93	3.03	3.929(5)	163.1
C(18)-H(18)···Br(2)#3	0.93	2.97	3.876(5)	163.7
C(19)-H(19A)···Br(2)#2	0.97	2.96	3.786(4)	144.1
O(1^a)-H(1A^a)···Br(3)	0.82	2.81	3.498(9)	143.4
Symmetry transformations used to generate equivalent atoms: #1 -*x*+1, *y*, -*z*+3/2, #2 *x*, -*y*+1, *z*-1/2, #3 -*x*+3/2, *y*+1/2, -*z*+3/2				
1·MeCN-Br				
C(2)-H(2)···Br(2)#2	0.93	3.02	3.915(4)	161.9
C(6)-H(6)···N(1^a)#3	0.93	2.63	3.191(14)	119.3
C(18)-H(18)···Br(2)#4	0.93	3.00	3.905(4)	164.5
C(19)-H(19A)···Br(2)#2	0.97	3.04	3.860(4)	142.7
C(22^a)-H(22B^a)···Br(1)#4	0.96	2.89	3.689(16)	141.5
Symmetry transformations used to generate equivalent atoms: #1 -*x*+1, *y*, -*z*+3/2, #2 *x*+1/2, *y*-1/2, *z*, #3 -*x*+3/2, -*y*+3/2, -*z*+1, #4 -*x*+1, -*y*+1, -*z*+1, #5 -*x*+1, *y*, -*z*+1/2				

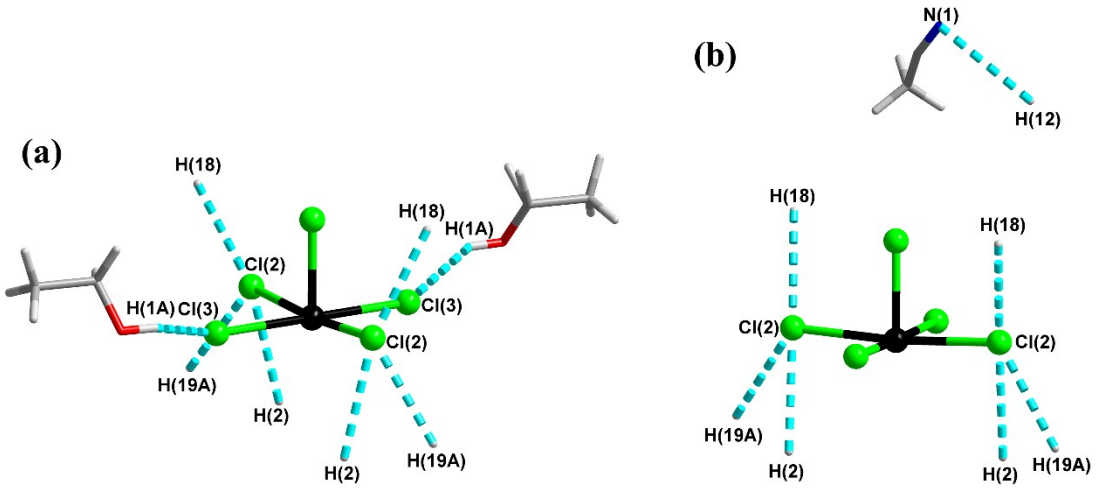

Figure S14. Hydrogen bonds of **1·EtOH-Cl** (**a**) and **1·MeCN-Cl** (**b**). Black ball, Sb; green ball, Cl; blue ball, N; red ball, O; dark gray ball, C; light gray ball, H. Turquoise dotted lines represent hydrogen bonds.

Table S6. Hydrogen bonds for **1·EtOH-Cl** at 293 K and **1·MeCN-Cl** at 295 K.

D-H···A	d(D-H)	d(H···A)	d(D···A)	<(DHA)
1·EtOH-Cl				
C(2)-H(2)···Cl(2)#2	0.93	2.89	3.789(4)	162.7
C(18)-H(18)···Cl(2)#3	0.93	2.83	3.729(4)	162.2
C(19)-H(19A)···Cl(2)#2	0.97	2.85	3.670(4)	142.2
O(1^a)-H(1A^a)···Cl(3)	0.85	2.71	3.440(8)	144.5
Symmetry transformations used to generate equivalent atoms: #1 -*x*+1,-*y*+1,-*z*, #2 -*x*+2,-*y*+1,-*z*+1				
1·MeCN-Cl				
C(2)-H(2)···Cl(2)#2	0.93	2.90	3.803(3)	163.1
C(6)-H(6)···N(1^a)#3	0.93	2.67	3.190(13)	116.2
C(18)-H(18)···Cl(2)#4	0.93	2.86	3.761(3)	163.7
C(19)-H(19A)···Cl(2)#2	0.97	2.93	3.737(3)	141.4
Symmetry transformations used to generate equivalent atoms: #1 -*x*+1,*y*,-*z*+3/2, #2 *x*+1/2,*y*-1/2,*z*, #3 -*x*+3/2,-*y*+3/2,-*z*+1,#4 -*x*+1,-*y*+1,-*z*+1				

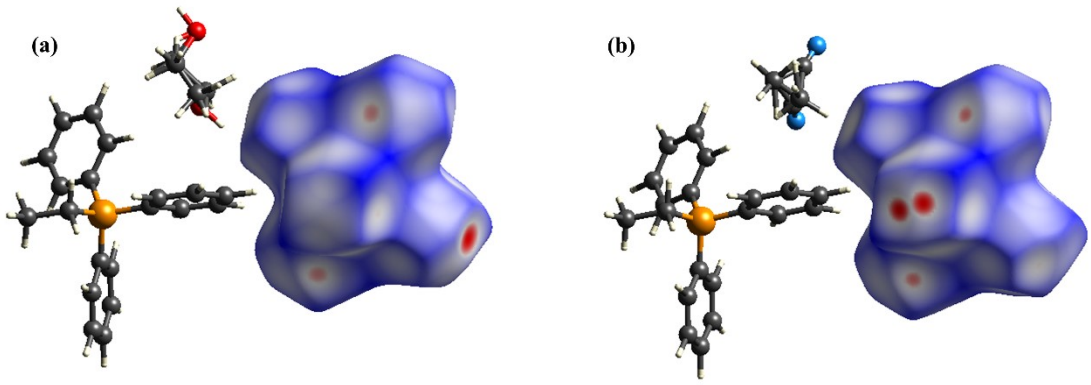

Figure S15. The Hirshfeld d_{norm} surfaces of inorganic part with all interactions for **1·EtOH-Br** (**a**)

and **1·MeCN-Br** (**b**). The highlights in red represent closer distances and stronger interactions while white and blue highlights refer to longer distances and weak interactions.

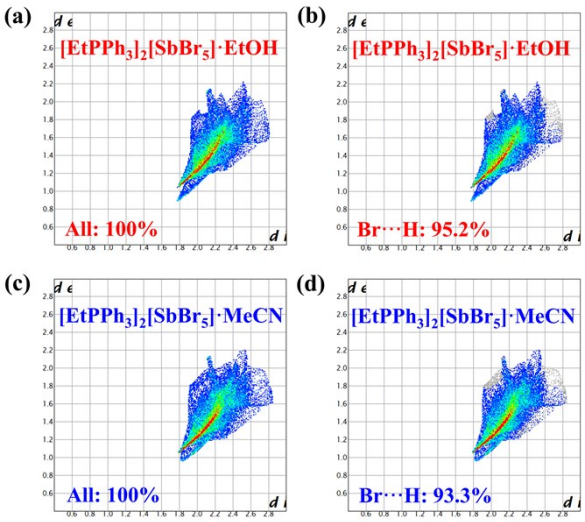

Figure S16. The 2D fingerprint plots for **1·EtOH-Br** and **1·MeCN-Br**. All weak interactions for **1·EtOH-Br** (**a**) and **1·MeCN-Br** (**c**) are 100%. The contribution of Br···H hydrogen bonds is 95.2% and 93.3% for **1·EtOH-Br** (**b**) and **1·MeCN-Br** (**d**), respectively.

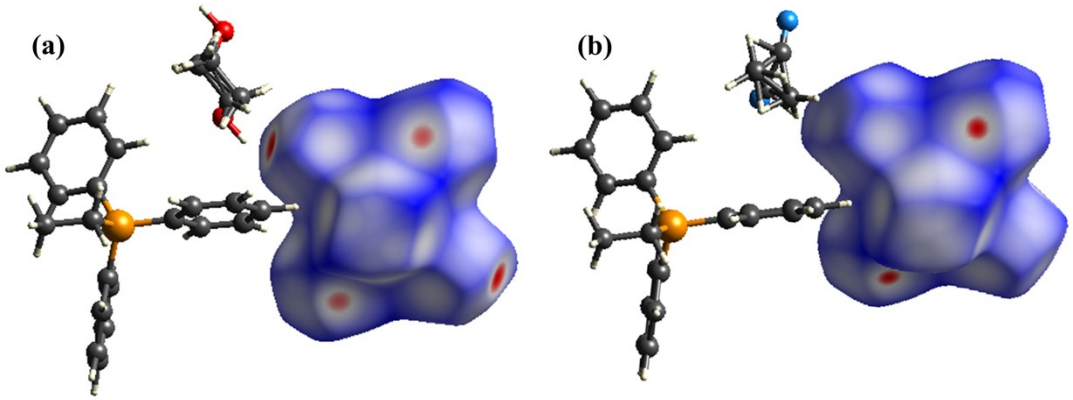

Figure S17. The Hirshfeld d_{norm} surfaces of inorganic part with all interactions for **1·EtOH-Cl** (**a**) and **1·MeCN-Cl** (**b**). The highlights in red represent closer distances and stronger interactions while white and blue highlights refer to longer distances and weak interactions.

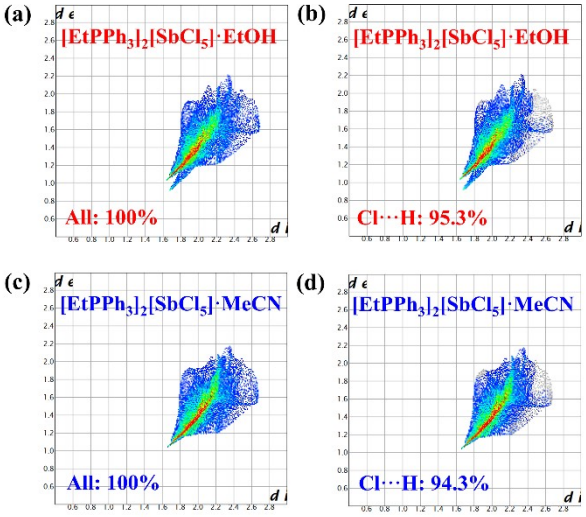

Figure S18. The 2D fingerprint plots for **1·EtOH-Cl** and **1·MeCN-Cl**. All weak interactions for **1·EtOH-Cl** (**a**) and **1·MeCN-Cl** (**c**) are 100%. The contribution of Cl···H hydrogen bonds is 95.3% and 94.3% for **1·EtOH-Cl** (**b**) and **1·MeCN-Cl** (**d**), respectively.